iScience

CellPress
OPEN ACCESS

Article

Matrix Pore Size Governs Escape of Human Breast Cancer Cells from a Microtumor to an Empty Cavity

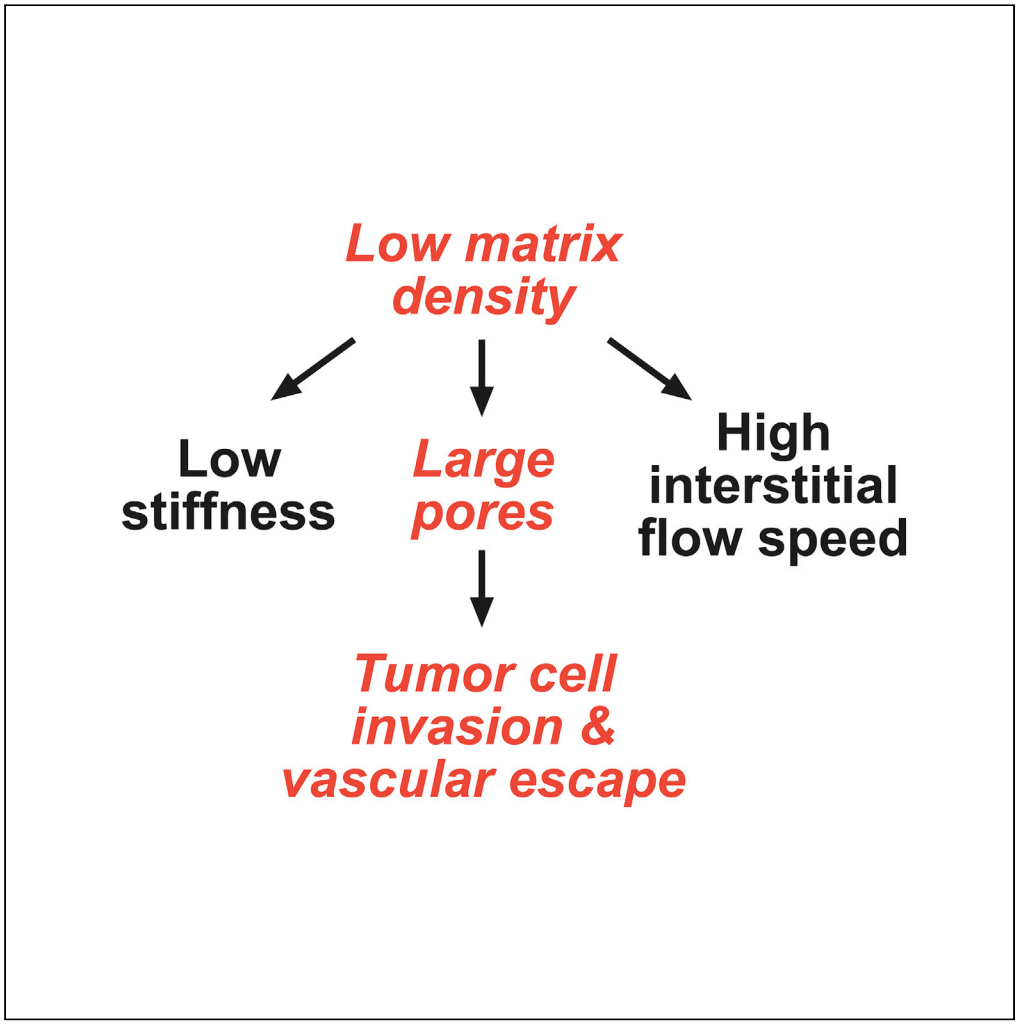

Joe Tien, Usman Ghani, Yoseph W. Dance, Alex J. Seibel, M. Çağatay Karakan, Kamil L. Ekinci, Celeste M. Nelson

jtien@bu.edu (J.T.)
celesten@princeton.edu (C.M.N.)

HIGHLIGHTS

Dense collagen matrix slows escape of MDA-MB-231 human breast cancer cells

The effect of collagen density correlates best with the pore size of the matrix

Matrix stiffness and interstitial flow speed have little effect on tumor cell escape

Tien et al., iScience *23*, 101673
November 20, 2020
https://doi.org/10.1016/j.isci.2020.101673

iScience

CellPress
OPEN ACCESS

Article

Matrix Pore Size Governs Escape of Human Breast Cancer Cells from a Microtumor to an Empty Cavity

Joe Tien,[1,2,7,*] Usman Ghani,[1] Yoseph W. Dance,[1] Alex J. Seibel,[1] M. Çağatay Karakan,[3,4] Kamil L. Ekinci,[2,3,4] and Celeste M. Nelson[5,6,*]

SUMMARY

How the extracellular matrix (ECM) affects the progression of a localized tumor to invasion of the ECM and eventually to vascular dissemination remains unclear. Although many studies have examined the role of the ECM in early stages of tumor progression, few have considered the subsequent stages that culminate in intravasation. In the current study, we have developed a three-dimensional (3D) microfluidic culture system that captures the entire process of invasion from an engineered human micro-tumor of MDA-MB-231 breast cancer cells through a type I collagen matrix and escape into a lymphatic-like cavity. By varying the physical properties of the collagen, we have found that MDA-MB-231 tumor cells invade and escape faster in lower-density ECM. These effects are mediated by the ECM pore size, rather than by the elastic modulus or interstitial flow speed. Our results underscore the importance of ECM structure in the vascular escape of human breast cancer cells.

INTRODUCTION

The extracellular matrix (ECM) plays a crucial role in the progression of a solid tumor from a localized growth to frank metastasis (Liotta, 2016; Lu et al., 2012). This role is mediated in part by the ability of tumor and stromal cell-surface receptors to bind directly to the ECM, as well as to growth factors and other molecules that are sequestered within the ECM. The specific three-dimensional (3D) presentation of these ligands by the ECM to the cell surface tailors the resulting signaling response and can alter whether a tumor cell remains in place or ultimately invades (Radisky et al., 2002). Recent studies have also established that flow of interstitial fluid within the ECM can generate chemotactic gradients and flow-induced mechanotransduction that alter the direction of tumor cell movement (Haessler et al., 2012; Pisano et al., 2015; Polacheck et al., 2014; Shields et al., 2007).

Aside from tuning signaling, the ECM also provides a 3D physical space for tumor progression, and the physical properties of the ECM affect the rate of tumor cell migration from the initial lesion to a nearby blood or lymphatic vessel. Of the many different physical parameters that describe the ECM, the ones that are best appreciated for their effects on tumor progression are stiffness and pore size. In breast cancer, ECM cross-linking (which increases stiffness) synergizes with mammary epithelial cell transformation to promote local invasion, whereas less cross-linking results in lower-grade tumors (Levental et al., 2009). Migration of tumor cells through the ECM appears to depend more on pore size than on stiffness, with small and large pore sizes favoring protease-dependent and -independent migration, respectively (Petrie et al., 2017; Wolf et al., 2013); similar pore size-dependent migration has been observed through synthetic constrictions of different sizes (Davidson et al., 2014; Harada et al., 2014). Proteolytic resistance and the orientation of ECM fibers also affect tumor cell behavior (Provenzano et al., 2006; Zaman et al., 2006). Much of the progress in this field has been obtained through the use of 3D *in vitro* models of tumor cell growth and invasion, particularly those that use hydrogels of reconstituted type I collagen as the ECM (Guzman et al., 2014; Wolf et al., 2009). The ability to control the structure of the collagen network through changes in collagen concentration and/or gelation conditions (temperature, pH, ionic strength) has made it possible to vary the physical properties of these ECMs systematically and even to match them to those of tumors *in vivo* (Raviraj et al., 2012).

[1]Department of Biomedical Engineering, Boston University, Boston, MA 02215, USA

[2]Division of Materials Science and Engineering, Boston University, Boston, MA 02215, USA

[3]Department of Mechanical Engineering, Boston University, Boston, MA 02215, USA

[4]Photonics Center, Boston University, Boston, MA 02215, USA

[5]Department of Chemical and Biological Engineering, Princeton University, Princeton, NJ 08554, USA

[6]Department of Molecular Biology, Princeton University, Princeton, NJ 08554, USA

[7]Lead Contact

*Correspondence: jtien@bu.edu (J.T.), celesten@princeton.edu (C.M.N.)

https://doi.org/10.1016/j.isci.2020.101673

Although much is now known about how the physical state of the ECM affects the initial stages of tumor progression, how it affects the subsequent migration and escape of tumor cells into the lumens of nearby vasculature remains poorly studied. Compared with local invasion, the steps that culminate in intravasation are difficult to image *in vivo* and model *in vitro*. Invasion and vascular dissemination are distinct, and increased local invasion does not necessarily lead to increased dissemination (Padmanaban et al., 2019). As a result, many questions remain open about the role of the ECM in tumor cell dissemination. For instance, are there stage-specific effects of ECM on invasion and intravasation? Which factor is more important for successful escape of the tumor cell: ECM stiffness, pore size, or something else entirely? Does interstitial flow within the ECM guide tumor cells toward the vascular lumen? Given that it is the vascular dissemination of tumor cells that results in seeding of distant organs, it is important to understand how the ECM affects this stage and not just how it affects the initial stage of invasion.

The current study represents a first step toward answering these questions, by examining how the physical properties of a type I collagen gel affect the escape of MDA-MB-231 human triple-negative breast cancer cells from a pre-formed dense aggregate through the gel and into a lymphatic-like cavity. The culture model that this study uses is based on one that we developed to observe the invasion of breast cancer cells from an aggregate into a collagen gel under interstitial flow, which mimics the initial stage of breast tumor progression (Piotrowski-Daspit et al., 2016; Tien et al., 2012). The current study extends the existing model to intravasation by incorporating a cavity into which the tumor cells can escape. Because the cavity is not lined by endothelial cells, ECM-specific effects can be isolated from potential confounding signals from the endothelium. By altering the stiffness and pore size of the collagen gel and the magnitude of interstitial flow through the gel, we have found that pore size is the main physical factor that determines the rate at which MDA-MB-231 cells escape into the cavity.

RESULTS

To investigate how the physical properties of the ECM affect cancer cell escape, we used a microfluidic-based strategy to engineer microtumors of MDA-MB-231 cells within a type I collagen gel (Figure S1). This strategy afforded us the opportunity to vary the 3D network structure of the ECM around the tumors. Tumors were formed adjacent to empty cavities that were designed to mimic the blind end of a lymphatic vessel. Without lymphatic endothelial cells in the system, any changes in tumor cell behavior can be attributed to direct and indirect effects of changes in the ECM properties. Movement of cancer cells through the collagen and into the empty cavity was tracked over a period of 16 days.

Lower Collagen Concentration Promotes Microtumor Escape

To determine how ECM density affects cancer cell escape, we generated microtumors in collagen gels that were formed at 37°C in two different concentrations (Figure 1). When surrounded by low-density collagen (2.5 mg/mL), cancer cells invaded from the tumors even before flow was applied on day 2 (Figure 1, "*Day 2*"). In contrast, when surrounded by high-density collagen (3.9 mg/mL), invasions only appeared after the application of flow. Tumors in high-density collagen invaded primarily as multicellular collectives, whereas those in low-density collagen also invaded as single cells (Figure 1, "*Day 5*"). In both formulations of collagen, cells from the tumors invaded the ECM, migrated toward the cavity, and entered the cavity (i.e., escaped). Eventually, cells filled the cavity, most likely through local proliferation within the cavity and/or migration of trailing cells into the cavity (Figure 1, "*Day 14*"). All tumors were maintained at least until they escaped, or until day 16 if they did not escape.

To compare the kinetics of invasion and escape in low- and high-density collagen, we represented the temporal data using Kaplan-Meier survival plots. Although all microtumors developed invasions within 5 days of inducing flow (i.e., by day 7), invasions emerged sooner from those in low-density collagen ($p < 0.0001$; Figure 2A). Standard survival-curve analysis showed that the hazard ratio (HR) for invasion in low-density collagen was 25, with 95% confidence interval (CI) of 14–43. Escape also occurred sooner in low-density collagen, with roughly half of those tumors escaping by day 6 ($p < 0.0001$; HR, 3.8; 95% CI, 2.5–5.9; Figure 2B).

The initial distance *D* (as measured on day 0) between the tips of a tumor and its opposing cavity represents the minimum length of ECM that must be traversed for a tumor cell to escape (Figure 2C). As a result, we anticipated that this distance would play a dominant role on the rate of escape, and the distributions of *D* were matched for the different experimental conditions (Figure S2A). We then grouped the tumors into

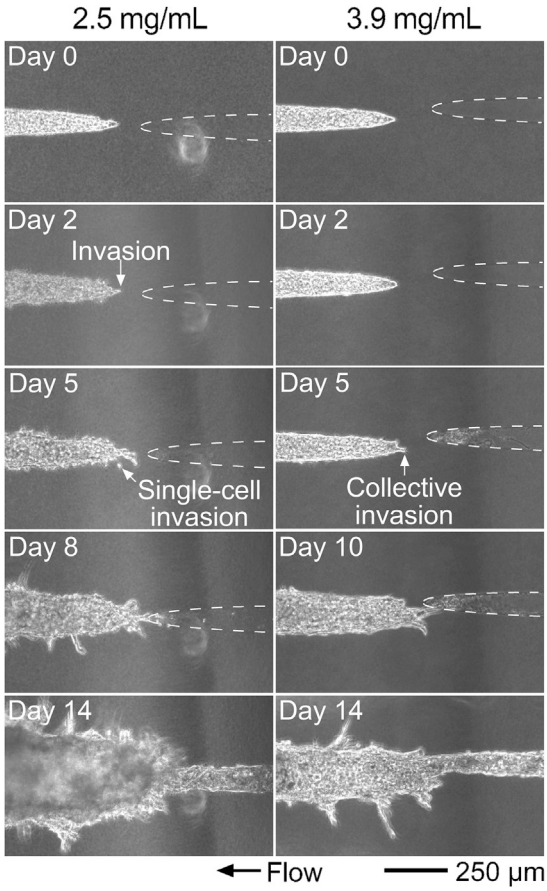

Figure 1. Time-Lapse Images of Tumor Progression in Low-Density (2.5 mg/mL) and High-Density (3.9 mg/mL) Collagen

Tumors progressed from a well-outlined boundary to invasion to escape into the cavity. Dotted lines outline the cavities. Flow started on day 2, and is from right to left.

"low" ($D < 150$ μm) and "high" (150 μm < $D < 300$ μm) categories; tumors with $D > 300$ μm never escaped by day 16, and we did not analyze this group further. Low-D tumors escaped sooner in low-density collagen than in high-density collagen ($p < 0.0001$; HR, 5.3; 95% CI, 2.6–11; Figure 2D), and high-D tumors behaved similarly ($p < 0.0001$; HR, 4.2; 95% CI, 2.4–7.4; Figure 2E). As expected, cells escaped faster from low-D tumors compared with high-D tumors in both low- ($p < 0.0001$) and high-density collagen ($p = 0.0001$).

To better understand how collagen concentration affects the rate of escape, we plotted the tumor-to-cavity distances for each tumor over time (Figures 3A and 3B). These plots showed no evidence for acceleration (or deceleration) of tumors toward the cavity, and we used a linear fit to determine the speed of movement for each tumor from its day of invasion onward. These speeds do not necessarily represent the rate of individual cell migration but rather provide the overall rate at which a tumor approaches its opposing cavity. We found that tumors in low-density collagen moved faster toward the cavity than those in high-density collagen did ($p < 0.0001$; Figure 3C). This finding indicates that cancer cells escape sooner in low-density collagen not only because invasions arise earlier but also because tumors move faster toward the cavity.

ECM Permeability Controls Tumor Escape

To identify the physical features that mediate the effect of ECM concentration on cancer cell escape, we measured the indentation moduli and permeabilities of the different collagen gels. Not surprisingly, we found that low-density collagen had a higher Darcy permeability ($p < 0.0001$; Figure S3A) and a lower elastic modulus ($p < 0.0001$; Figure S3B) than high-density collagen did. Scanning electron microscopy showed that the average pore area of low-density collagen (0.038 ± 0.002 μm^2) was larger than that of

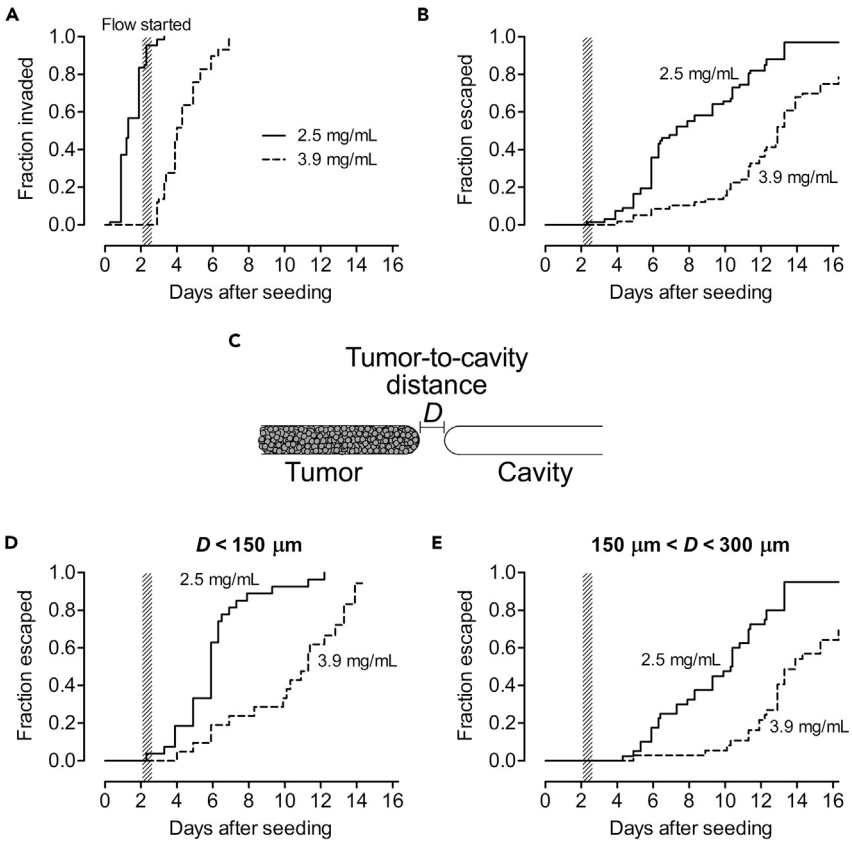

Figure 2. Invasion and Escape of Cancer Cells from Tumors in Low- and High-Density Collagen

(A) Kaplan-Meier plots of invasion in the collagen gels. 2.5 mg/mL: *n* = 67 (none censored); 3.9 mg/mL: *n* = 58 (none censored).

(B) Kaplan-Meier plots of escape in the collagen gels. 2.5 mg/mL: *n* = 67 (2 censored); 3.9 mg/mL: *n* = 58 (15 censored).

(C) Schematic diagram that defines the tumor-to-cavity distance *D*.

(D) Kaplan-Meier plots of escape in low-*D* tumors. 2.5 mg/mL: *n* = 27 (none censored); 3.9 mg/mL: *n* = 21 (2 censored).

(E) Kaplan-Meier plots of escape in high-*D* tumors. 2.5 mg/mL: *n* = 40 (2 censored); 3.9 mg/mL: *n* = 37 (13 censored).

high-density collagen (0.027 $\pm$ 0.006 μm^2; p = 0.035) (Figure S3C), a result that is consistent with the larger permeability of the low-density gel. To parse the relative effects of permeability (or pore size) and stiffness on cancer cell escape, we generated tumors in gels that displayed the permeability of low-density collagen but the stiffness of high-density collagen. Varying the temperature of gelation has been found to alter the elastic modulus of collagen gels independently of collagen concentration (Yang et al., 2009). Trial-and-error variations of gelation temperature and collagen concentration showed that 3.2 mg/mL collagen gels that were formed at 12°C had the desired permeability and stiffness; their average pore area of 0.047 $\pm$ 0.006 μm^2 was statistically indistinguishable from that of 2.5 mg/mL gels (p = 0.097) and was larger than that of 3.9 mg/mL gels (p = 0.0019) (Figure S3). We repeated the escape experiments with this collagen formulation, while ensuring that the tumor-to-cavity distance distributions were matched between conditions (Figure S2B).

In the 3.2 mg/mL (12°C) collagen, invasions started to appear even before flow was applied, and single-cell invasions were observed in these gels (Figure 4). These observations are similar to those in the low-density (2.5 mg/mL) collagen. Indeed, invasion occurred at similar rates in the two collagen formulations (p = 0.20; Figure 5A). Escape in 3.2 mg/mL (12°C) collagen also occurred at a similar rate to that in low-density collagen (p = 0.26; Figure 5B). Compared with tumors in high-density (3.9 mg/mL) collagen, tumors in 3.2 mg/mL (12°C) collagen invaded (p < 0.0001; HR, 42; 95% CI, 20–89; Figure 5A) and escaped (p < 0.0001; HR, 4.3; 95% CI, 2.4–7.9; Figure 5B) sooner. The speeds of tumor movement toward the cavity in 3.2 mg/mL (12°C) collagen were similar to those in low-density collagen (p = 1.0) but greater than in

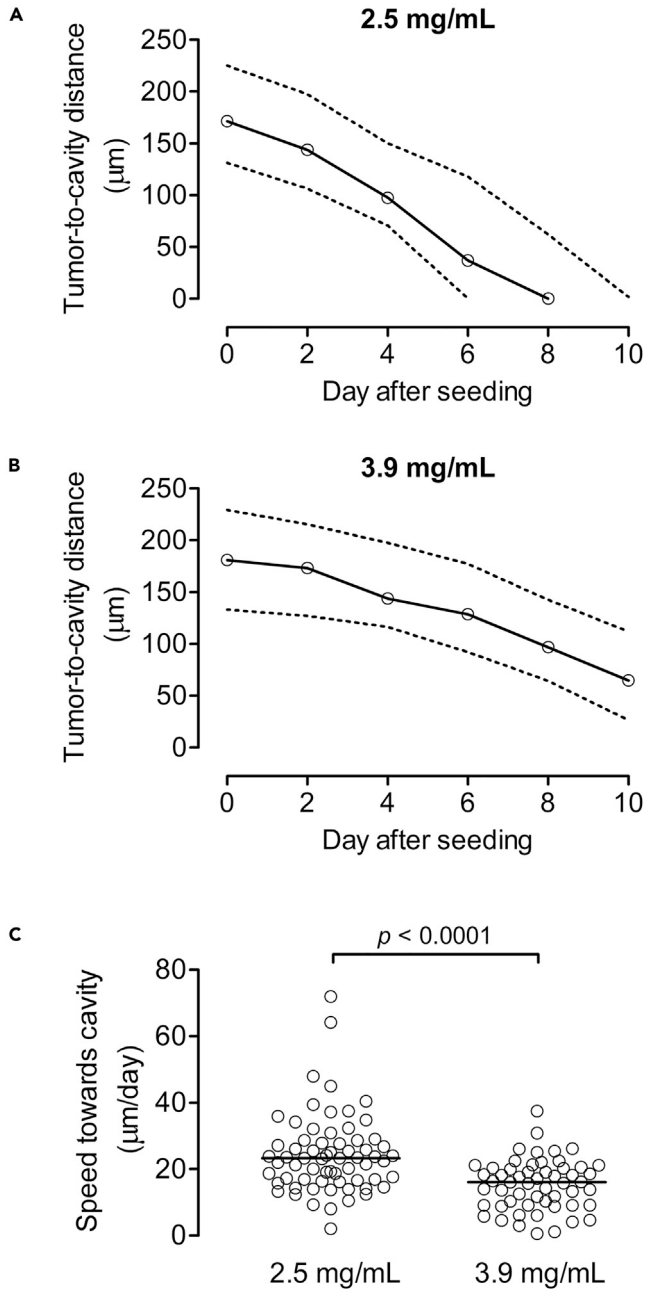

Figure 3. Tumor-to-Cavity Movement in Low- and High-Density Collagen

(A and B) Tumor-to-cavity distances as a function of time, in (A) low-density and (B) high-density collagen. Solid lines represent median values; dotted lines represent 25th and 75th percentiles. Bars represent medians.

(C) Tumor-to-cavity speeds, measured after tumors had invaded.

high-density collagen (p = 0.018) (Figure 5C). By design, 3.2 mg/mL (12°C) and low-density collagen gels have the same permeabilities and pore areas but different moduli, whereas 3.2 mg/mL (12°C) and high-density collagen gels have the same moduli but different permeabilities and pore areas. Taken together, our results demonstrate that the rates of invasion and escape correlate with the permeability and pore area, and not the elastic modulus, of the ECM.

The Darcy permeability of the collagen measures the resistance of the ECM to fluid flow. Thus, changes in permeability also affect the rate of fluid flow experienced by the tumor, with higher permeabilities resulting

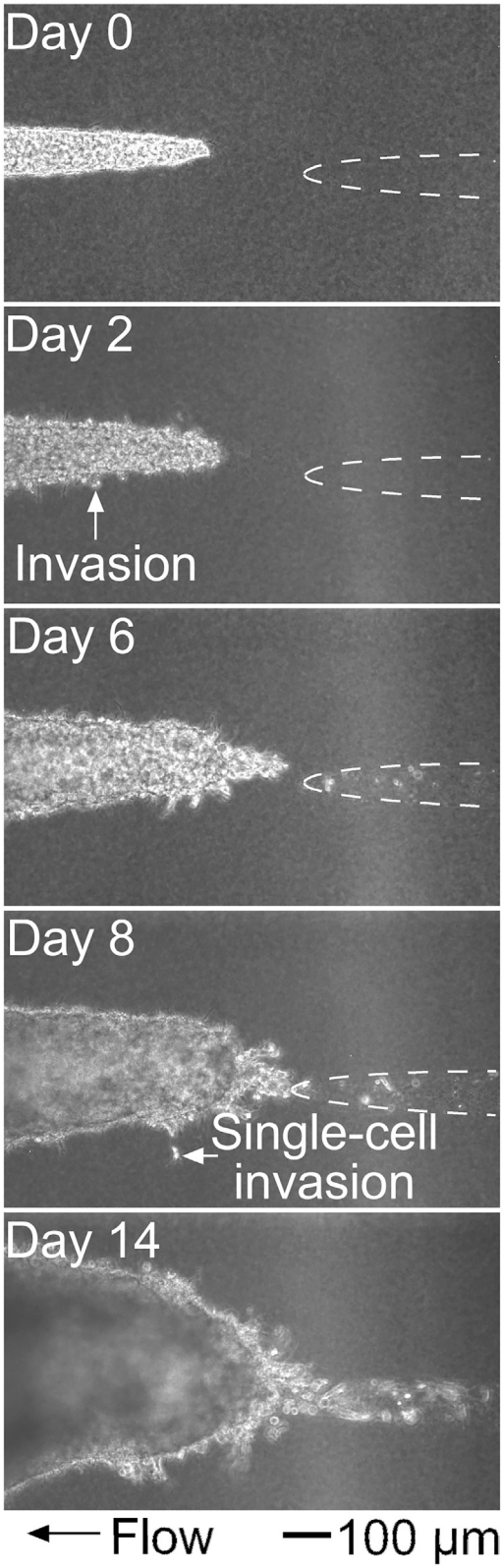

Figure 4. Time-Lapse Images of Tumor Progression in 3.2 mg/mL (12°C) Collagen

Tumors progressed from a well-outlined boundary to invasion to escape into the cavity. Dotted lines outline the cavities. Flow started on day 2, and is from right to left.

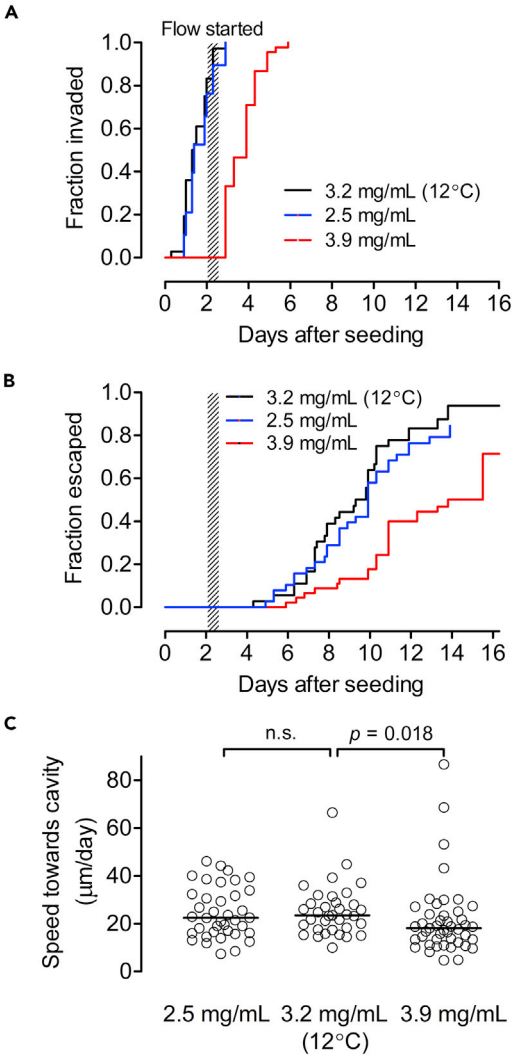

Figure 5. Invasion and Escape of Cancer Cells from Tumors in 2.5, 3.9, and 3.2 mg/mL (12°C) Collagen

(A) Kaplan-Meier plots of invasion. 2.5 mg/mL: *n* = 38 (none censored); 3.9 mg/mL: *n* = 45 (none censored); 3.2 mg/mL (12°C): *n* = 36 (none censored).

(B) Kaplan-Meier plots of escape. 2.5 mg/mL: *n* = 38 (7 censored); 3.9 mg/mL: *n* = 45 (20 censored); 3.2 mg/mL (12°C): *n* = 36 (4 censored).

(C) Tumor-to-cavity speeds, measured after tumors had invaded. Bars represent medians.

in higher flow rates for the same driving pressure difference. Given that interstitial flow has been shown to affect migration of MDA-MB-231 cells (Haessler et al., 2012; Polacheck et al., 2011; Shields et al., 2007), we tested whether the effects of ECM permeability on escape were mediated by changes in interstitial flow. Since flow rates in these tumors decreased over time as the pressure head dissipated between the twice-daily feedings (Figure S4A, *inset*), the initial flow rates (i.e., the ones measured immediately after re-feeding) represent the maximum flow rates across a tumor. As expected, tumors in low-density collagen experienced a higher initial flow rate than those in high-density collagen did ($p < 0.0001$; Figure S4A). We then subjected tumors in low- and high-density collagen to low and high flow rates, respectively, by changing the heights of the applied hydrostatic pressures (Figure S4A). Again, distributions of tumor-to-cavity distance were matched for each condition (Figure S2C). Even when cultured under low initial flow rates, tumors in low-density collagen still invaded sooner than those in high-density collagen did ($p < 0.0001$; HR, 24; 95% CI, 9.9–60; Figure 6A). Similar results were found when tumors in both collagen formulations were subjected to high initial flow rates ($p < 0.0001$; HR, 30; 95% CI, 12–75; Figure 6A). Escape was

earlier as well in low-density collagen under low flow ($p = 0.0040$; HR, 2.9; 95% CI, 1.4–5.8; Figure 6B) or high flow ($p < 0.0001$; HR, 5.3; 95% CI, 2.4–11; Figure 6B). For a given collagen concentration, tumors under low and high initial flow advanced toward the cavity with equivalent speeds (Figure 6C). With matched flow rates, tumors still moved faster toward the cavity in low-density collagen than in high-density collagen ($p = 0.0054$; Figure 6D). These data indicate that the differences in tumor behavior observed in low-density (high permeability and pore area) and high-density (low permeability and pore area) collagen were not driven mainly, if at all, by differences in the initial flow rates.

DISCUSSION

The current study examines how the invasion and escape of MDA-MB-231 triple-negative human breast cancer cells are affected by the concentration of the ECM that surrounds the tumor. Our main findings are: (1) a low collagen concentration hastens tumor invasion and escape and increases the speed with which a tumor moves toward a lymphatic-like cavity; (2) these effects of collagen concentration are mediated by the permeability, and not the elastic modulus, of the ECM; and (3) the magnitude of interstitial flow through the ECM does not affect invasion or escape. Given that the Darcy permeability of a porous material is a measure of the average pore radius squared and that permeability correlated with pore area in these gels, our results strongly suggest the increase in invasion and escape at lower collagen concentrations is a structural effect that stems from the larger pores found at these concentrations. Below, we discuss these findings in the context of previous studies that have examined how the physical properties of the ECM affect breast tumor progression.

It is well appreciated that tumor progression is regulated in part by the elastic modulus of the surrounding ECM, with stiffer ECM promoting invasion (Butcher et al., 2009). Given that we did not find an effect of collagen modulus on tumor invasion, how can these findings be reconciled? In earlier studies, stiffening of the ECM resulted from cross-linking of polyacrylamide gel substrata or from overexpression of lysyl oxidase, an endogenous cross-linker of collagen and other ECM proteins (Levental et al., 2009; Paszek et al., 2005). Moreover, the breast epithelial cells that were used for invasion assays were either non-malignant (primary human mammary epithelial cells, immortalized MCF-10A cells) or dysplastic (ErbB2-expressing MCF-10A cells). In contrast, we and many others have used highly invasive MDA-MB-231 cells in type I collagen gels, with the elastic modulus of the ECM controlled by altering gelation conditions instead of by chemical cross-linking. These differences in cell type and ECM preparation may lead to the different results obtained here and in previous studies. In particular, MDA-MB-231 cells were originally derived from pleural effusions and thus represent a far more invasive and migratory breast cancer cell than MCF-10A cells and their derivatives (Cailleau et al., 1974). It is possible that MDA-MB-231 cells are sufficiently invasive that any effect of ECM modulus on invasion of this cell type is comparatively small. Since the current study only examines the behavior of MDA-MB-231 cells, our conclusion that ECM modulus plays at most a minor role in tumor cell escape is limited to this cell line.

Quantitative differences in the elastic moduli for the culture substrata used in the current and previous studies may also account for discordances in invasion. Although the indentation moduli of the gels used here (200–400 Pa) are lower than those reported at the invasive front of invasive ductal carcinoma (Acerbi et al., 2015), they lie within the 100- to 1,200-Pa range used in previous *in vitro* studies (Levental et al., 2009; Paszek et al., 2005). One should keep in mind that these moduli were measured using different approaches (e.g., bulk indentation versus AFM) and on gels in different formats.

Our results are more consistent with previous work that used MDA-MB-231 cells for studies of invasion and migration (Guzman et al., 2014; Wolf et al., 2013). These studies found that ECM modulus had no consistent effect, and instead that the average pore size determined the rate at which cells invaded and migrated in 3D collagenous ECM. In the current study, we found that ECM permeability is the dominant physical property in tumor invasion and escape. The Darcy permeability is approximately equal to the average pore radius squared in 3D fibrous structures with high porosity (Jackson and James, 1986), such as the collagen gels used here (porosity >99%), which implies pore diameters of ~0.44, ~0.86, and ~0.89 μm in 3.9, 2.5, and 3.2 mg/mL (12°C) gels, respectively; the ordering of these values is consistent with that obtained from SEM images. Thus, our finding that ECM permeability controls tumor cell behavior is congruent with the conclusions of these previous studies.

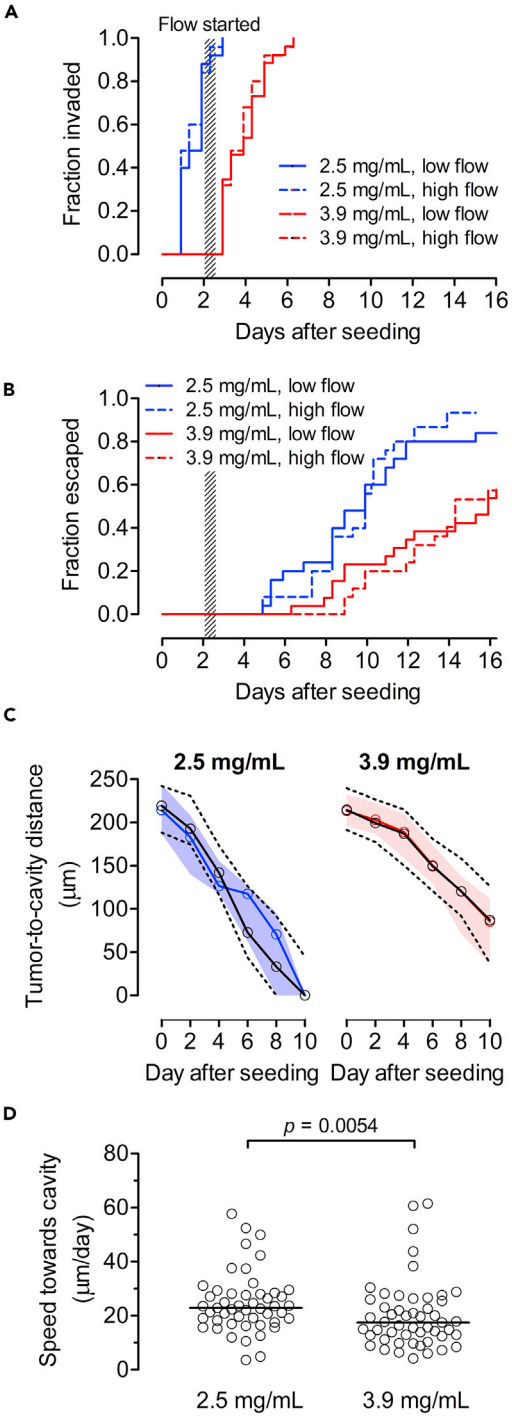

Figure 6. Invasion and Escape of Cells from Tumors in Low- and High-Density Collagen under Low and High Initial Flow

(A) Kaplan-Meier plots of invasion. 2.5 mg/mL, low flow: $n = 25$ (none censored); 2.5 mg/mL, high flow: $n = 25$ (none censored); 3.9 mg/mL, low flow: $n = 26$ (none censored); 3.9 mg/mL, high flow: $n = 25$ (none censored).

(B) Kaplan-Meier plots of escape. 2.5 mg/mL, low flow: $n = 25$ (4 censored); 2.5 mg/mL, high flow: $n = 25$ (3 censored); 3.9 mg/mL, low flow: $n = 26$ (11 censored); 3.9 mg/mL, high flow: $n = 25$ (11 censored).

Figure 6. *Continued*

(C) Tumor-to-cavity distances as a function of time, in (*left*) low-density and (*right*) high-density collagen. Black solid lines represent median values, and black dotted lines represent 25th and 75th percentiles, for tumors under low flow. Blue or red lines and shading represent the median values and 25th-to-75th percentile ranges, respectively, for tumors under high flow.

(D) Tumor-to-cavity speeds, measured after tumors had invaded. Data from low- and high-flow tumors are pooled. Bars represent medians.

It is important to recognize that the pore sizes within these gels are smaller than the size of an individual cell. They are also smaller than the average pore sizes for the dilute (0.3–1.7 mg/mL) collagen gels used in previous work, in which the migration of MDA-MB-231 cells was protease-independent and could proceed through ameboid movement (Wolf et al., 2013). In our system, invasion and escape of MDA-MB-231 cells require protease-mediated degradation (Rabie et al., unpublished results), which is consistent with the smaller pore size of the gels used here. The pore sizes shown in the SEM images in Figure S3C resemble those from mammographically dense tissue (Raviraj et al., 2012).

We found that the tumor cells migrated to the cavity as multicellular streams in low- and high-density collagen and also as single cells in low-density collagen only. These findings are consistent with those reported for other types of cancer cells (fibrosarcoma, melanoma) and can also be attributed to the effects of ECM permeability and pore size (Haeger et al., 2014). Others have reported that ECM density can modulate how spheroids of tumor cells invade through an "unjamming transition" (i.e., fluidization of the cell cluster) and its accompanying morphological changes (Ilina et al., 2020).

Despite several reports that interstitial flow can affect the migration of MDA-MB-231 cells in collagen gels (Haessler et al., 2012; Polacheck et al., 2011; Shields et al., 2007), we did not find any dependence of tumor cell escape or tumor movement speed on the magnitude of interstitial flow. When matching flows across different gel conditions (Figure S4A), we used the initial flow rate (i.e., immediately after re-feeding a tumor), which measures the flow speed integrated across the cross-sectional area of a tumor and its surrounding gel. To obtain a local measure of the flow that is experienced at the surface of a tumor, we used finite-element models to simulate the flow profile in different gel conditions (Figure S4B). The computed flow speeds at the surface of the tumor nearest to a cavity (located 200 μm away) were 2.6 μm/s for 3.9 mg/mL gels and 3.9 μm/s for 2.5 and 3.2 mg/mL (12°C) gels, which are comparable with the interstitial flow speeds (up to 4.6 μm/s) applied in the more recent studies of Kamm and Swartz (Haessler et al., 2012; Polacheck et al., 2011, 2014). Although the previous studies used the identical cell and ECM types as we used here, the collagen concentrations in the previous work were lower (1.5–2 mg/mL) than those here. As a result, we expect the pore sizes in previous studies to be larger than in our experiments, which may alter the role of interstitial flow in driving cell migration. The unsteady nature of the flow in our tumors, which results from dissipation of the pressure head between the twice-daily media replacement times, also contrasts with the steadier flows in previous studies.

Our results show that MDA-MB-231 tumor cell invasion and escape are governed by the same physical properties of the ECM. Both of their rates are controlled mainly by ECM permeability (and pore size) and not by the elastic modulus or initial flow rate. Thus, in this model of human breast cancer progression, the ECM serves primarily as a physical barrier to escape. It is notable that the ~4-fold difference in permeability (and accompanying difference in average pore size) between low- and high-density collagen is sufficient to alter the rate of escape substantially, with hazard ratios of four or more. The results of this study suggest that, at least for MDA-MB-231 cells, breast tumor cell escape, the immediate precursor to vascular dissemination, is particularly sensitive to the pore size of the ECM and that one strategy to reduce the rate of metastatic escape *in vivo* may be to decrease the average pore size in the tumor interstitium.

Limitations of the Study

This study has several limitations that should be kept in mind when interpreting the relevance of the findings to human breast cancer. First, the experiments were performed with only one breast cancer cell line (MDA-MB-231) and the conclusions obtained here may not necessarily hold for other cell lines or for human breast tumors *in vivo*. Second, the cavities into which the cancer cells escaped were not lined with endothelial cells, unlike actual vessels into which escape occurs during intravasation *in vivo*. Third, no stromal cells (mammary fibroblasts, adipocytes) were present within the collagen. Fourth, the interstitial flow was unsteady, with a period of 10–14 h.

Resource Availability

Lead Contact

Further information and requests for resources and reagents should be directed to and will be fulfilled by the Lead Contact, Joe Tien (jtien@bu.edu).

Materials Availability

This study did not generate new unique reagents.

Data and Code Availability

The datasets generated during this study are available upon reasonable request.

METHODS

All methods can be found in the accompanying Transparent Methods supplemental file.

SUPPLEMENTAL INFORMATION

Supplemental Information can be found online at https://doi.org/10.1016/j.isci.2020.101673.

ACKNOWLEDGMENTS

We thank Derek Radisky for helpful discussions and Anlee Krupp for technical assistance. Y.W.D. was supported by the National Institute of General Medical Sciences under award T32 GM008764 and through the CURE Diversity Research Supplements Program at the National Cancer Institute. This work was supported by grants from the National Cancer Institute (CA187692, CA214292) and a Faculty Scholars Award from the Howard Hughes Medical Institute.

AUTHOR CONTRIBUTIONS

U.G., Y.W.D., A.J.S., and M.C.K. performed experiments. All authors analyzed the data. J.T., U.G., and C.M.N. wrote the manuscript. J.T. and C.M.N. supervised the study.

DECLARATION OF INTERESTS

The authors declare no competing interests.

Received: June 28, 2020
Revised: October 2, 2020
Accepted: October 8, 2020
Published: November 20, 2020

REFERENCES

Acerbi, I., Cassereau, L., Dean, I., Shi, Q., Au, A., Park, C., Chen, Y.Y., Liphardt, J., Hwang, E.S., and Weaver, V.M. (2015). Human breast cancer invasion and aggression correlates with ECM stiffening and immune cell infiltration. Integr. Biol. *7*, 1120–1134.

Butcher, D.T., Alliston, T., and Weaver, V.M. (2009). A tense situation: forcing tumour progression. Nat. Rev. Cancer *9*, 108–122.

Cailleau, R., Young, R., Olivé, M., and Reeves, W.J., Jr. (1974). Breast tumor cell lines from pleural effusions. J. Natl. Cancer Inst. *53*, 661–674.

Davidson, P.M., Denais, C., Bakshi, M.C., and Lammerding, J. (2014). Nuclear deformability constitutes a rate-limiting step during cell migration in 3-D environments. Cell Mol. Bioeng. *7*, 293–306.

Guzman, A., Ziperstein, M.J., and Kaufman, L.J. (2014). The effect of fibrillar matrix architecture on tumor cell invasion of physically challenging environments. Biomaterials *35*, 6954–6963.

Haeger, A., Krause, M., Wolf, K., and Friedl, P. (2014). Cell jamming: collective invasion of mesenchymal tumor cells imposed by tissue confinement. Biochim. Biophys. Acta *1840*, 2386–2395.

Haessler, U., Teo, J.C.M., Foretay, D., Renaud, P., and Swartz, M.A. (2012). Migration dynamics of breast cancer cells in a tunable 3D interstitial flow chamber. Integr. Biol. *4*, 401–409.

Harada, T., Swift, J., Irianto, J., Shin, J.-W., Spinler, K.R., Athirasala, A., Diegmiller, R., Dingal, P.C.D.P., Ivanovska, I.L., and Discher, D.E. (2014). Nuclear lamin stiffness is a barrier to 3D migration, but softness can limit survival. J. Cell Biol. *204*, 669–682.

Ilina, O., Gritsenko, P.G., Syga, S., Lippoldt, J., La Porta, C.A.M., Chepizhko, O., Grosser, S., Vullings, M., Bakker, G.-J., Starruß, J., et al. (2020). Cell-cell adhesion and 3D matrix confinement determine jamming transitions in breast cancer invasion. Nat. Cell Biol. *22*, 1103–1115.

Jackson, G.W., and James, D.F. (1986). The permeability of fibrous porous media. Can J. Chem. Eng. *64*, 364–374.

Levental, K.R., Yu, H., Kass, L., Lakins, J.N., Egeblad, M., Erler, J.T., Fong, S.F.T., Csiszar, K., Giaccia, A., Weninger, W., et al. (2009). Matrix crosslinking forces tumor progression by enhancing integrin signaling. Cell *139*, 891–906.

Liotta, L.A. (2016). Adhere, degrade, and move: the three-step model of invasion. Cancer Res. *76*, 3115–3117.

Lu, P., Weaver, V.M., and Werb, Z. (2012). The extracellular matrix: a dynamic niche in cancer progression. J. Cell Biol. *196*, 395–406.

Padmanaban, V., Krol, I., Suhail, Y., Szczerba, B.M., Aceto, N., Bader, J.S., and Ewald, A.J. (2019). E-cadherin is required for metastasis in multiple models of breast cancer. Nature *573*, 439–444.

Paszek, M.J., Zahir, N., Johnson, K.R., Lakins, J.N., Rozenberg, G.I., Gefen, A., Reinhart-King, C.A., Margulies, S.S., Dembo, M., Boettiger, D., et al. (2005). Tensional homeostasis and the malignant phenotype. Cancer Cell *8*, 241–254.

Petrie, R.J., Harlin, H.M., Korsak, L.I.T., and Yamada, K.M. (2017). Activating the nuclear piston mechanism of 3D migration in tumor cells. J. Cell Biol. *216*, 93–100.

Piotrowski-Daspit, A.S., Tien, J., and Nelson, C.M. (2016). Interstitial fluid pressure regulates collective invasion in engineered human breast tumors *via* Snail, vimentin, and E-cadherin. Integr. Biol. *8*, 319–331.

Pisano, M., Triacca, V., Barbee, K.A., and Swartz, M.A. (2015). An *in vitro* model of the tumor-lymphatic microenvironment with simultaneous transendothelial and luminal flows reveals mechanisms of flow enhanced invasion. Integr. Biol. *7*, 525–533.

Polacheck, W.J., Charest, J.L., and Kamm, R.D. (2011). Interstitial flow influences direction of tumor cell migration through competing mechanisms. Proc. Natl. Acad. Sci. U S A *108*, 11115–11120.

Polacheck, W.J., German, A.E., Mammoto, A., Ingber, D.E., and Kamm, R.D. (2014). Mechanotransduction of fluid stresses governs 3D cell migration. Proc. Natl. Acad. Sci. U S A *111*, 2447–2452.

Provenzano, P.P., Eliceiri, K.W., Campbell, J.M., Inman, D.R., White, J.G., and Keely, P.J. (2006). Collagen reorganization at the tumor-stromal interface facilitates local invasion. BMC Med. *4*, 38.

Radisky, D., Muschler, J., and Bissell, M.J. (2002). Order and disorder: the role of extracellular matrix in epithelial cancer. Cancer Invest. *20*, 139–153.

Raviraj, V., Fok, S., Zhao, J., Chien, H.-Y., Lyons, J.G., Thompson, E.W., and Soon, L. (2012). Regulation of ROCK1 via Notch1 during breast cancer cell migration into dense matrices. BMC Cell Biol. *13*, 12.

Shields, J.D., Fleury, M.E., Yong, C., Tomei, A.A., Randolph, G.J., and Swartz, M.A. (2007). Autologous chemotaxis as a mechanism of tumor cell homing to lymphatics via interstitial flow and autocrine CCR7 signaling. Cancer Cell *11*, 526–538.

Tien, J., Truslow, J.G., and Nelson, C.M. (2012). Modulation of invasive phenotype by interstitial pressure-driven convection in aggregates of human breast cancer cells. PLoS One *7*, e45191.

Wolf, K., Alexander, S., Schacht, V., Coussens, L.M., von Andrian, U.H., van Rheenen, J., Deryugina, E., and Friedl, P. (2009). Collagen-based cell migration models in vitro and in vivo. Semin. Cell Dev. Biol. *20*, 931–941.

Wolf, K., te Lindert, M., Krause, M., Alexander, S., te Riet, J., Willis, A.L., Hoffman, R.M., Figdor, C.G., Weiss, S.J., and Friedl, P. (2013). Physical limits of cell migration: control by ECM space and nuclear deformation and tuning by proteolysis and traction force. J. Cell Biol. *201*, 1069–1084.

Yang, Y.-l., Leone, L.M., and Kaufman, L.J. (2009). Elastic moduli of collagen gels can be predicted from two-dimensional confocal microscopy. Biophys. J. *97*, 2051–2060.

Zaman, M.H., Trapani, L.M., Sieminski, A.L., Mackellar, D., Gong, H., Kamm, R.D., Wells, A., Lauffenburger, D.A., and Matsudaira, P. (2006). Migration of tumor cells in 3D matrices is governed by matrix stiffness along with cell-matrix adhesion and proteolysis. Proc. Natl. Acad. Sci. U S A *103*, 10889–10894.

iScience, Volume *23*

Supplemental Information

Matrix Pore Size Governs Escape of Human Breast Cancer Cells from a Microtumor to an Empty Cavity

Joe Tien, Usman Ghani, Yoseph W. Dance, Alex J. Seibel, M. Çağatay Karakan, Kamil L. Ekinci, and Celeste M. Nelson

SUPPLEMENTAL INFORMATION

Transparent Methods

Figure S1. Schematic diagram of the formation of invasive tumors with empty cavities in a type I collagen gel. Related to Figures 1, 2, 3, 4, 5, and 6.

Figure S2. Relative frequency distributions of initial (day 0) tumor-to-cavity distances *D*. Related to Figures 2, 3, 5, and 6.

Figure S3. Physical properties of the collagen gels. Related to Figures 4 and 5.

Figure S4. Measured and computed flows in and around tumors. Related to Figure 6.

TRANSPARENT METHODS

Cell culture

MDA-MB-231 human breast carcinoma cells (Physical Sciences-Oncology Network Bioresource Core Facility, ATCC) were cultured in DMEM/F12 medium (Hyclone) that was supplemented with 10% heat-inactivated fetal bovine serum (FBS, lot #B18020; Atlanta Biologicals) and 50 μg/mL gentamicin (Sigma). Cells were passed 1:4 every four days and discarded after passage 15.

Formation of microtumors

Figure S1 shows the procedure for forming the microtumors (n = 344). Bovine dermal type I collagen (4.9 mg/mL, acid-extracted, lot #210090; Koken) was neutralized and diluted with 10× Hanks' balanced salt solution (HBSS; Invitrogen), cell culture medium, 0.2 M NaOH, and water to a pH of 9-9.5, a final collagen concentration of 2.5, 3.2, or 3.9 mg/mL, and a final FBS concentration of 0.4%. A silicone (PDMS) chamber that contained a recessed feature was oxidized and then placed feature-side down on a glass coverslip to define a 1 mm × 1 mm × 6 mm rectangular channel that was open at both ends. The channel was immediately coated with poly-D-lysine (1 mg/mL in H_2O; Sigma) for one hour to promote adhesion of the gel. Two 120-μm-diameter needles were coated with 1% bovine serum albumin (BSA) for at least one hour and threaded into the rectangular channel from opposite sides of the PDMS chamber. For 2.5 and 3.9 mg/mL gels, collagen solution was added and then gelled for at least twenty-five minutes at 37°C around the needles. For the 3.2 mg/mL gels, the solution was gelled for six hours at 12°C and then held at room temperature for at least twenty-five minutes. Cell culture medium was added to the 6-mm-diameter wells on either end of the channel, and the needles were removed to yield two opposing cavities in the gel. Gels were conditioned overnight with cell culture medium.

The next day, one cavity was seeded with a suspension of MDA-MB-231 cells (~10^6 cells per mL) for 15-20 minutes to form a ~3-mm-long microtumor. The adjacent well was then washed with medium to remove excess cells. For the first two days after seeding, each microtumor was fed every 10-14 hours by removing medium from the two wells and adding fresh culture medium, with a slight excess

added to the well adjacent to the microtumor. On day 2, a stack of PDMS spacers was placed on top of the well next to the empty cavity and filled with culture medium to apply a hydrostatic pressure head of 3.5 to 11 mm H_2O; this pressure condition induced fluid to flow from the cavity to the tumor and is permissive for cell invasion (Tien et al., 2012). The tumors were fed once every 10-14 hours for an additional fourteen days (i.e., to day 16) by adding medium to the upstream PDMS stack and removing the medium that had collected in the downstream well.

Starting on day 0 (i.e., on the day of seeding), phase-contrast images were acquired daily on an Axiovert 200 inverted microscope (Zeiss) with a 10×/0.30 *NA* Plan-Neofluar objective and an Axiocam MRm camera (Zeiss) at 1388 × 1040 resolution. The tumor-to-cavity separation distance D was calculated as $\sqrt{D_{xy}^{\,2} + D_z^{\,2}}$ where D_{xy} was the two-dimensional separation distance measured in the image and D_z was the difference in the heights of the tumor and cavity planes. All values of D_z were corrected by a factor of 1.33 to account for the index of refraction of the fluid (Cox, 2012).

Microtumor invasion and escape assay

Tumors were examined twice per day by phase-contrast microscopy. A tumor was considered to have "invaded" when at least one cell body was observed to be located at least 20 μm from the initial boundary of the tumor. It was considered to have "escaped" when at least one cell body was observed within the cavity opposite the tumor. Tumors that had not escaped by the end of day 16 (i.e., fourteen days after application of flow) were discarded and considered to be censored in subsequent Kaplan-Meier analysis. Occasionally, MDA-MB-231 cells grew along the PDMS-gel or glass-gel interface; these tumors were censored if and when the cells obstructed the view of the cavity.

We considered an invasion to be multicellular when it clearly consisted of two or more cells that formed an invasive strand that was contiguous with the tumor. Single-cell invasion refers to a single cell that was clearly isolated within the gel. Ambiguous cases were considered invasion without definitively establishing whether the invasion was multicellular or consisted of a single cell.

Measurement of tumor-to-cavity movement speed

For every microtumor, the shortest distance between any tumor cell and the cavity was measured every two days, starting on day 0. If escape had occurred, then the distance was zero. A linear regression of the distance versus time yielded the average speed of tumor movement towards the empty cavity. Only distances that were obtained between the days of invasion and escape, inclusive, were used for regression.

Measurement of initial flow rates

The volumes of fluid gain and loss in the downstream and upstream wells of a microtumor, respectively, were measured three hours after feeding. The average of the two values was taken to correct for evaporation, and then divided by the time from the previous feeding (i.e., three hours) to obtain the initial flow rate. Flow rates were measured on day 4.

Measurement of collagen permeability

Solid gels (6 mm in length) were formed using the same type of PDMS chambers as that used for the microtumors, but without needles. A stack of PDMS spacers that was filled with culture medium was used to apply a pressure difference across the gel. We measured the volume of medium that flowed through the gel in 1-5 hours at 37°C. The Darcy permeability K of the gel was calculated using the formula $K = Q\mu L/A\Delta P$, where Q is the flow rate, μ is the viscosity of culture medium (found to be 0.72 cPoise at 37°C), L is the length of the gel, A is the cross-sectional area of the gel, and ΔP is the applied pressure difference.

Collagen indentation analysis

To measure the elastic moduli of the collagen gels, we cast neutralized collagen into a stack of PDMS spacers to form discs of gel 2 mm in height and 6 mm in diameter. After the gels were submerged in PBS, we placed a steel ball (2.0 mm in diameter; Precision Balls) on top of each gel and allowed it to

indent the gel for one hour. We measured the resulting indentation and determined the elastic modulus E_{ind} of a gel using the equation $E_{ind} = \pi R^{5/2}(\rho - \rho_{PBS})g/\delta^{3/2}$, where R is the radius of the ball (1.0 mm), ρ is the density of steel (8 g/cm^3), ρ_{PBS} is the density of PBS, g is gravitational acceleration (9.8 m/s^2), and δ is the indentation depth.

Scanning electron microscopy (SEM)

Flat discs of collagen gel (1 mm in thickness, ~1 cm in diameter) were cast between glass slides and fixed overnight at room temperature in 2.5% glutaraldehyde (Electron Microscopy Sciences) in PBS. Fixed gels were washed three times with PBS, followed by three washes with deionized water. They were then dehydrated in a graded ethanol (EtOH) series (30-90% EtOH in 10% increments, followed by three washes in 100% EtOH) before being subjected to solvent exchange with hexamethyldisilazane (HMDS; Sigma) using a graded EtOH/HMDS series (2:1, 1:1, 1:2 mixtures of EtOH to HMDS, followed by three washes in 100% HMDS). Each step in gel washing, dehydration, and solvent exchange proceeded for at least fifteen minutes. Excess HMDS was removed, and gels were allowed to dry overnight. Dried gels were loaded on SEM stubs using carbon tape and sputter-coated with a ~10-nm-thick layer of Au/Pd. Images at 1024 × 768 resolution were obtained using a Supra 55VP or Supra 40VP field-emission SEM (Zeiss) at 3 kV accelerating voltage and 10,000× magnification. For each gel, the average pore area was calculated from the maximum inscribed circles in at least 100 pores in a 4×4 μm^2 field-of-view using ImageJ (NIH). Values are reported as mean ± SD for 3-4 gels per gelling condition.

Finite-element modeling of tumor flows

Flow within a tumor, its surrounding gel, and the opposing cavity was simulated using finite-element method-based models constructed in COMSOL Multiphysics ver. 5.4 (Comsol, Inc.). The tumor-to-cavity distance was set to 200 μm. Gels were modeled as porous media with Darcy permeabilities of 0.048 μm^2, 0.187 μm^2, or 0.2 μm^2 to match the experimentally measured values for 3.9 mg/mL, 2.5 mg/mL, or 3.2 mg/mL (12°C) collagen, respectively. Tumors were modeled as porous media

with an estimated Darcy permeability of 0.1 μm^2. Flow within cavities was treated as creeping flow, with a fluid viscosity of 0.72 cP. The flow profile for an applied pressure difference of 0.65 cm H_2O was computed using a PARDISO solver. Meshes were refined until a ~2-fold increase in model degrees-of-freedom resulted in a <2% change in the computed flow speed at the location on the tumor closest to the cavity.

Statistical analysis

All statistical tests were performed using Graphpad Prism ver. 6. Invasion and escape data were plotted as Kaplan-Meier curves. Single comparisons of two invasion or escape curves used the log-rank test. In these plots, "fraction invaded" and "fraction escaped" refer to the percentage of tumors that invaded or escaped, not to the percentage of cells that did so. Group comparisons of more than two invasion or escape curves used the log-rank test, followed by pairwise comparisons with a Bonferroni-corrected threshold for statistical significance of 0.025 (two comparisons) or 0.012 (four comparisons). Single comparison of tumor-to-cavity speeds used the Mann-Whitney *U* test. Group comparisons of tumor-to-cavity speeds, gel permeabilities, or indentation elastic moduli used the Kruskal-Wallis test, followed by Dunn's post-hoc test for selected pairwise comparisons. Group comparisons of average pore areas used one-way ANOVA, followed by Tukey's post-hoc test for pairwise comparisons. Except for pairwise comparisons of invasion or escape curves, the reported *p* values are already adjusted for any multiple comparisons and should be compared to a threshold of 0.05.

Reference

Cox, G. (2012). Optical Imaging Techniques in Cell Biology (Boca Raton, FL: CRC Press).

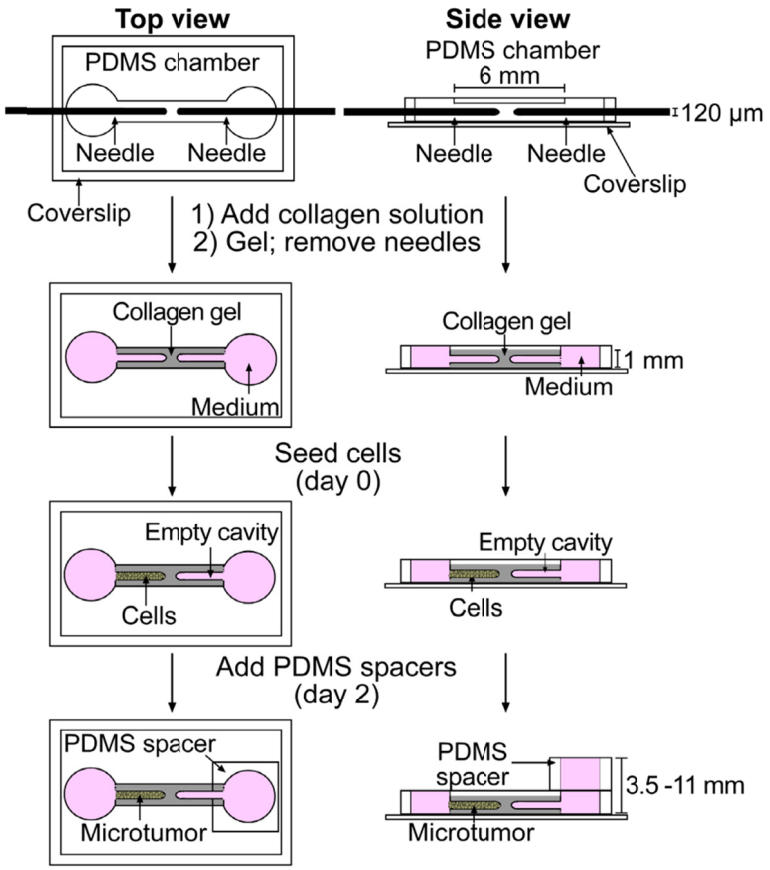

Figure S1. Schematic diagram of the formation of invasive tumors with empty cavities in a type I collagen gel. Related to Figures 1, 2, 3, 4, 5, and 6.

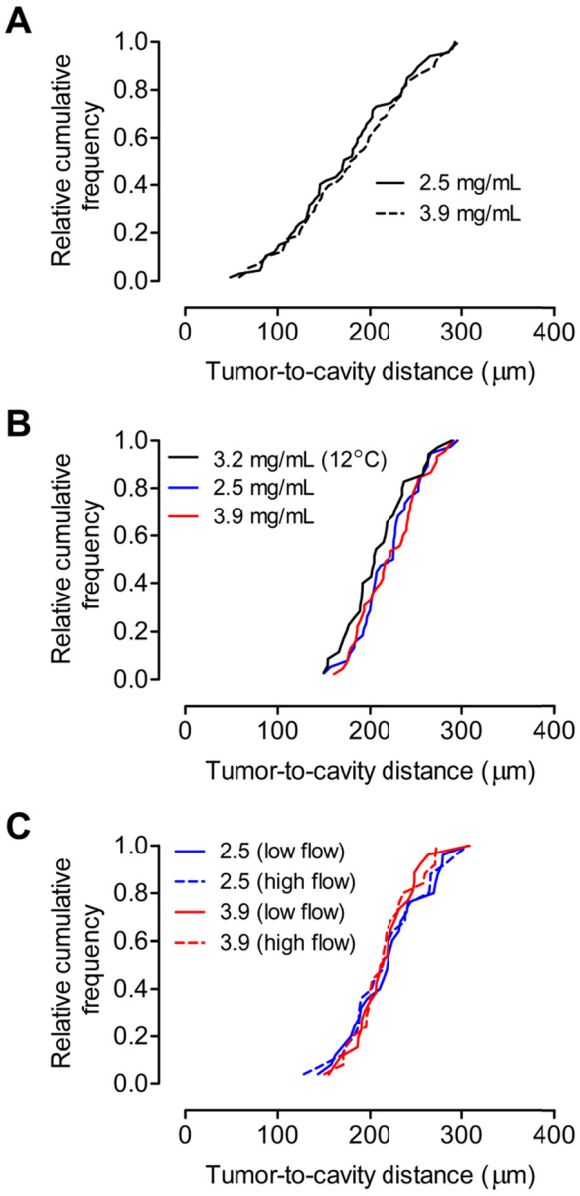

Figure S2. Relative frequency distributions of initial (day 0) tumor-to-cavity distances *D*. Related to Figures 2, 3, 5, and 6.

(A) Distributions for the tumors analyzed in Figures 2 and 3.

(B) Distributions for the tumors analyzed in Figure 5.

(C) Distributions for the tumors analyzed in Figure 6.

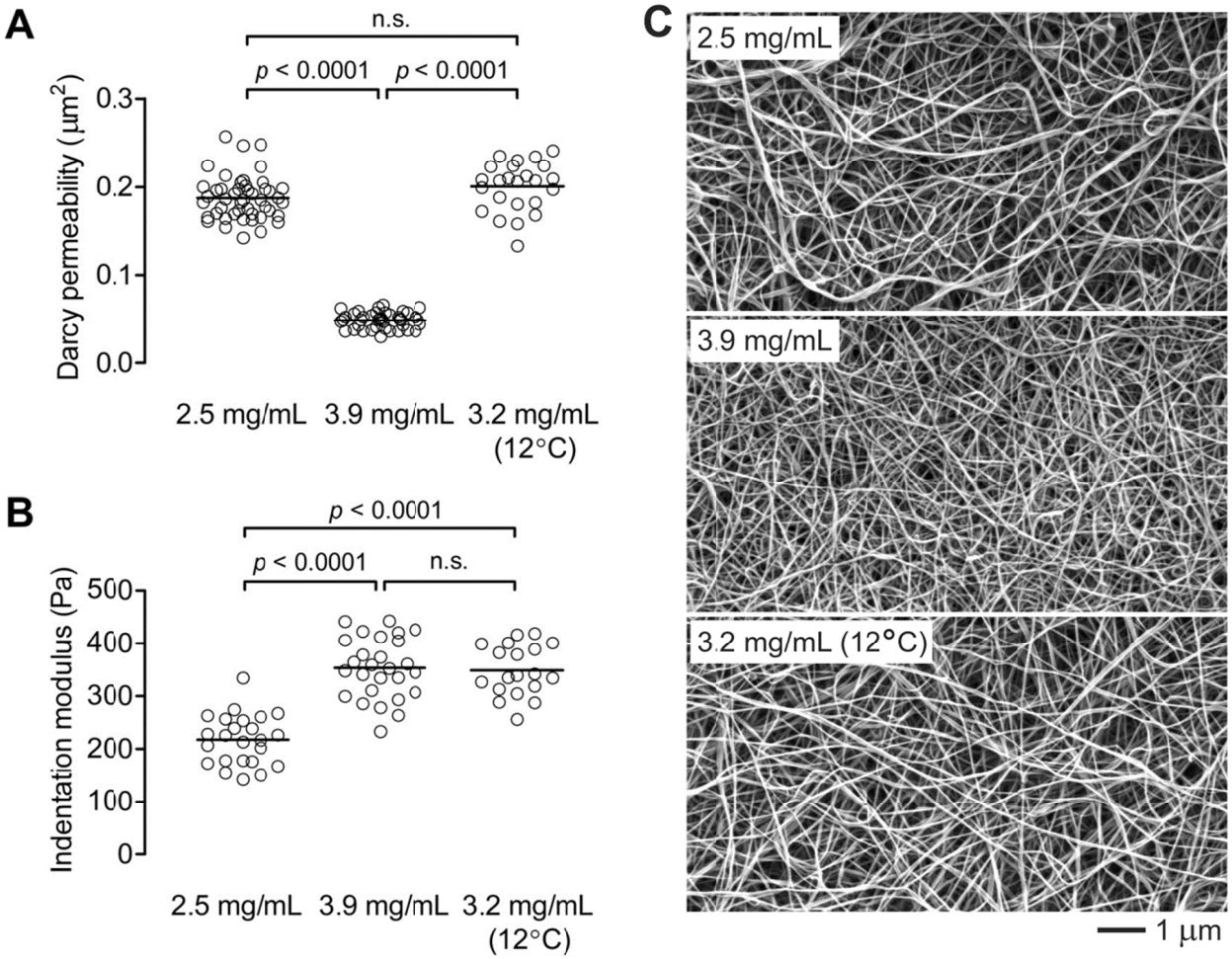

Figure S3. Physical properties of the collagen gels. Related to Figures 4 and 5.

(A) Darcy permeability. Bars represent means.

(B) Indentation modulus. Bars represent means.

(C) Representative SEM images.

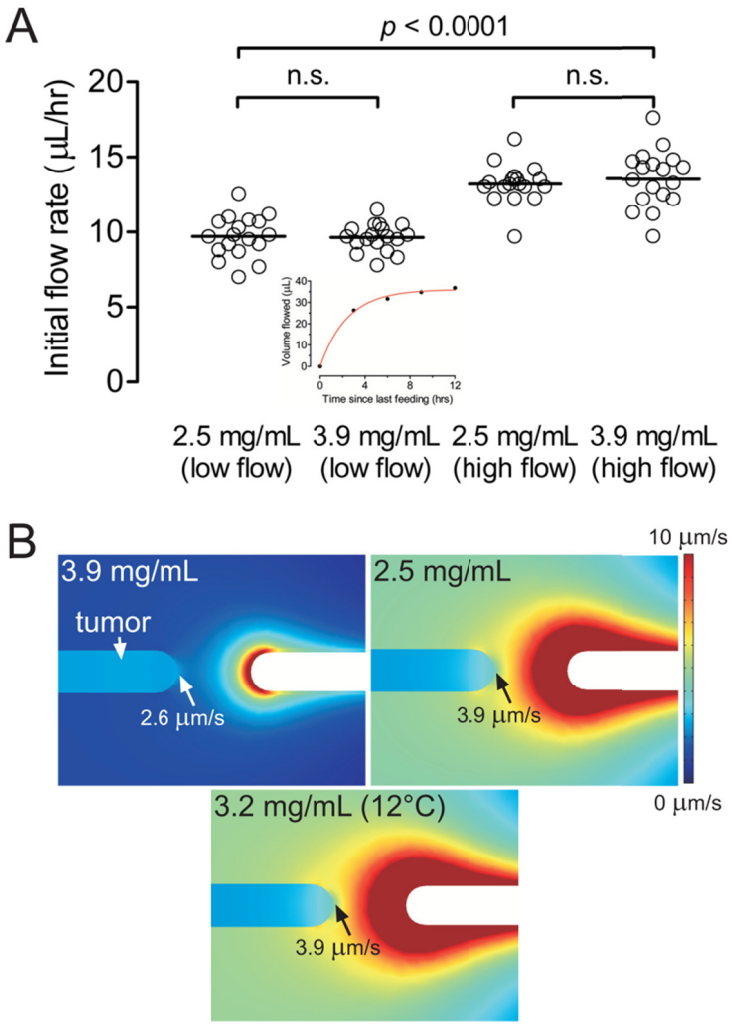

Figure S4. Measured and computed flows in and around tumors. Related to Figure 6.

(A) Measured initial flow rates for each combination of low- and high-flow condition and low- and high-density gel. Bars represent means. *Inset*, representative plot of cumulative flow volume versus time for a low-flow tumor in 3.9 mg/mL collagen; the red curve represents the best fit to an exponential decay with offset.

(B) Computed flow speeds in tumors and their surrounding gels, with a tumor-to-cavity separation of 200 µm. To enhance visualization of the speeds in and near tumors, the color scale is limited to a maximum speed of 10 µm/s.